Quantum condensation in electron–hole systems: excitonic BEC–BCS crossover and biexciton crystallization

2007 J. Phys.: Condens. Matter 19 295205

(http://iopscience.iop.org/0953-8984/19/29/295205)

IOP PUBLISHING JOURNAL OF PHYSICS: CONDENSED MATTER

J. Phys.: Condens. Matter **19** (2007) 295205 (20pp) doi:10.1088/0953-8984/19/29/295205

Quantum condensation in electron–hole systems: excitonic BEC–BCS crossover and biexciton crystallization

Tetsuo Ogawa, Yuh Tomio and Kenichi Asano

Department of Physics, Osaka University and CREST, JST, Toyonaka, Osaka 560-0043, Japan

Received 17 April 2007
Published 11 June 2007
Online at stacks.iop.org/JPhysCM/19/295205

Abstract

Quantum condensation of electron–hole (e–h) systems in photoexcited semiconductors is reviewed from a theoretical viewpoint, stressing the exciton Bose–Einstein condensation (BEC), the e–h BCS-type condensed state, the exciton Mott transition, and the biexciton crystallization. First, we discuss the crossover between the exciton BEC and the e–h BCS states at low temperature using the self-consistent t-matrix and local approximations, applied to the high-dimensional two-band Hubbard model with both repulsive and attractive on-site interactions. We also study the metal–insulator transition (called the 'exciton Mott transition') at zero and finite temperatures, investigated with the dynamical mean-field theory. Away from half-filling we find excitonic/biexcitonic insulating phases and the first-order transition between metallic and insulating states. Second, in a one-dimensional e–h system, we employ the exciton bosonization and renormalization-group techniques to clarify quantum orders at zero temperature. The most probable ground state exhibits the biexciton crystallization, which reflects the Tomonaga–Luttinger liquid properties, the e–h backward scattering, and the long-range Coulomb interaction. The one-dimensional e–h system is insulating even at the high-density limit, hence the exciton Mott transition never occurs at zero temperature in one dimension.

1. Introduction

For more than three decades, electron–hole (e–h) systems realized in photoexcited semiconductors have been intensively investigated both theoretically and experimentally [1], not only because the e–h systems govern optical properties of matter but also because various quantum cooperative phenomena are expected to take place depending on particle density, temperature and dimensionality [2, 3]. Several areas of interest in e–h systems arise. (i) What kind of quantum order is formed? (ii) How does such quantum order emerge in time and space? (iii) What are the optical responses, e.g. absorption, gain, photoluminescence, and nonlinear optical processes, of such quantum order like? In this paper we pay attention to

question (i). Here we shall define the term 'quantum order' in e–h systems. The e–h system is an *excited* state composed of two oppositely charged fermions, electrons and holes. Then this system is inherently nonequilibrium with a finite lifetime due to the interband recombination of nanosecond order. In usual inorganic semiconducting materials, e.g. GaAs, the intraband relaxation (of picosecond order) is much faster than the interband one (nanosecond order) [4]. In a timescale just after the photoexcitation and before the interband relaxation time, therefore, the system gets settled in a quasi-thermal-equilibrium state, where electrons and holes are approximately in (quasi)equilibrium at (quasi)temperature in each band. We here consider such a situation. Dynamical features of carrier relaxation processes in e–h systems are not treated in this paper. Note that the number of electrons is equal to that of holes in our definition of 'e–h systems'. Thus optical properties of initially *doped* semiconductors are out of this paper [5].

We shall guess intuitively what happens in an e–h system as the particle density increases, controlled by the excitation light intensity. In the low-density limit where only one electron and one hole are excited, an 'exciton' may be formed as a bosonic bound state of an electron and a hole [6]. Dimensionality dependence of excitons is also quite interesting [1, 7]. When two electrons and two holes are excited, a 'biexciton' (an excitonic molecule) is a possible bound state (also bosonic); this biexcitonic state reflects characteristics of the exciton–exciton interaction [8], and affects crucially the third-order optical nonlinearity of semiconductors [9]. Thus, how the optical responses of semiconductors depend on the number of excitons/biexcitons is a long-standing problem in the e–h physics.

In the case of stronger photoexcitation, where many electrons and holes are excited in semiconductors, many-body effects and the so-called electronic correlations should be taken carefully into account. In this case, macroscopic quantum phenomena, that is, e–h pair condensations, are expected, e.g. the Bose–Einstein condensation (BEC) of excitons [10–14] and the e–h superconductor-like state (e–h BCS state) [15, 16]. At very low temperature and at relatively low e–h particle density (strong-coupling regime), strongly bound e–h pairs undergo the BEC as an exciton gas. On the other hand, at high e–h density (weak-coupling regime) where the mean interparticle distance is shorter than the exciton Bohr radius, weakly bound e–h pairs may behave like the Cooper pairs in conventional superconductors at sufficiently low temperatures, that is, the Bardeen–Cooper–Schrieffer (BCS) state of e–h pairs. In the first half of this paper, we shall discuss these BEC and BCS states and the crossover with the use of the self-consistent t-matrix approximation and the local approximation, which are valid for the higher-dimensional systems.

Dissociation of many excitons (or biexcitons) into a gas state of electrons and holes (called the 'e–h plasma') may also be possible as the particle density further increases. This is called the 'exciton Mott transition' (insulator-to-metal transition). The main origins of this Mott transition are the Pauli blocking and enhancement of the Coulomb screening, which weaken the binding energy of the e–h bound states [2]. In the middle of this paper, details of the exciton Mott transition will be studied with the dynamical mean-field theory (DMFT) [17] for arbitrary particle density. The gas–liquid phase separation dynamics in an e–h plasma state [18–22] will not be discussed in this paper. In any case, the interparticle Coulomb interaction plays an essential role in the e–h problems.

In order to clarify the dimensionality of the e–h systems, we will investigate quantum orders in one-dimensional ($d = 1$) e–h systems. Since the simple perturbation theory based on the Fermi liquid picture [23] is not applicable to $d = 1$ systems, we employ the bosonization technique [24] and the renormalization-group method. From the theoretical point of view, $d = 1$ e–h systems are highly special, since in $d = 1$ an electron and a hole form an exciton bound state even when the attractive e–h interaction is infinitesimally weak. Therefore, we naively expect that the exciton Mott transition may be absent in $d = 1$. This argument

above, however, is insufficient since the Pauli blocking and dynamical screening effects are not considered. With increasing e–h particle density, the system goes to the weak-coupling regime, where the characteristic interaction energy is much smaller than the Fermi energies of electrons and holes. In this regime, hence, the bosonization method has advantages in that it can take full account of the interaction processes. We apply this technique to the $d = 1$ e–h system with the long-range Coulomb interaction in the last part of this paper. We will discuss the possibility of the biexciton liquid and crystal [25, 26] in $d = 1$ systems at absolute zero temperature.

This paper is organized as follows. In section 2, e–h quantum condensation at low temperature is discussed to clarify the crossover between the exciton BEC and the e–h BCS state. Section 3 is devoted to an analysis of the exciton Mott transition of normal (not pair condensed) phases of the e–h system. In both sections, we employ the two-band Hubbard model solved with a formalism of the dynamical mean-field theory (DMFT) combined with the t-matrix approximation, the local approximation, or the numerical exact diagonalization technique. The one-dimensional e–h system is analysed in section 4 by the bosonization and renormalization-group methods.

2. Exciton BEC and e–h BCS states in high-dimensional e–h systems

In this section, the crossover [27–30] between the exciton BEC and the e–h BCS-like state is studied to clarify differences from the BCS–BEC crossover in superconductors or trapped atomic Fermi gases [31–34]. Compared with other systems undergoing condensation of bound pairs, electrons and holes in quasi-thermal-equilibrium semiconductors have the following two notable characteristics: they have different effective masses and mass anisotropies [35, 36], and they involve not only the e–h attractive Coulomb interaction U' but also the repulsive one U between like particles besides the Pauli exclusion principle. In contrast to conventional superconductors, the attractive and repulsive interactions have the same energy scale. Therefore, we have to treat U and U' on an equal footing.

By calculating the condensation temperature T_c, we will clarify the effects of the repulsive interaction and the mass difference on the e–h pair condensation from the BCS to the BEC regime [37]. A simple two-band Hubbard model with attractive and repulsive on-site interactions is adopted to describe the e–h systems. Here we suppose that conduction electrons and valence holes, whose bands are isotropic, have infinite lifetime, and the number of electrons is equal to that of holes ($N_e = N_h$). In our model the interaction strengths and the particle density $n \equiv N_e/N = N_h/N$ are treated as independent parameters (where N is the total number of lattice sites). We employ the self-consistent t-matrix approximation (SCTMA) [38–40]. This approximation deals correctly with two-particle correlations. In addition to the SCTMA, we also use a local approximation (LA), which is justified in high spatial dimensions. The procedure is to neglect the momentum dependence of the self-energy and the vertex function. The SCTMA combined with the LA has been known to be successful for the superconductivity of the *single-band* attractive Hubbard model in high dimensions [40]. In particular, the successive interpolation between the BCS limit with $T_c \propto \exp(t/U')$ and the BEC limit with $T_c \propto t^2/U'$ can be described well [31, 32], where U' and t denote the attractive interaction and the transfer energy, respectively. Therefore, we extend the scheme to our two-band model, and expect that our results are valid for three-dimensional bulk systems.

2.1. The two-band Hubbard model and the self-consistent t-matrix approximation (SCTMA)

We start with the two-band Hubbard model to describe a many-body aspect of e–h systems:

$$\hat{H} = -\sum_{\langle ij\rangle,\sigma}\sum_{\nu=\mathrm{e,h}} t_\nu \hat{a}^{\nu\dagger}_{i\sigma}\hat{a}^{\nu}_{j\sigma} - \sum_{j\sigma,\nu}\mu_\nu \hat{n}^{\nu}_{j\sigma} + U\sum_{j,\nu}\hat{n}^{\nu}_{j\uparrow}\hat{n}^{\nu}_{j\downarrow} - U'\sum_{j\sigma\sigma'}\hat{n}^{\mathrm{e}}_{j\sigma}\hat{n}^{\mathrm{h}}_{j\sigma'}, \tag{1}$$

where $\hat{a}^{\mathrm{e}\dagger}_{j\sigma}$ ($\hat{a}^{\mathrm{h}\dagger}_{j\sigma}$) denotes a creation operator of an electron (a hole) with spin $\sigma = \{\uparrow, \downarrow\}$ at the jth site and $\hat{n}^{\nu}_{j\sigma} = \hat{a}^{\nu\dagger}_{j\sigma}\hat{a}^{\nu}_{j\sigma}$ with $\nu = \{e, h\}$. The quantities t_e (t_h) and μ_e (μ_h) are the transfer integral of the electrons (holes) between the nearest-neighbour sites and the chemical potential measured from the centre of the bare electron (hole) band, respectively. The on-site Coulomb interaction of the e–e (h–h) repulsion and that of the e–h attraction are expressed by U and $-U'$, respectively.

We apply the SCTMA to the model (1). Feynman diagrams contributing to the self-energy of electrons and holes in the normal phase within the SCTMA are shown in figure 1, where all the particle–hole and particle–particle ladder diagrams are taken into account with respect to the interaction U and $-U'$. The explicit expression of the self-energy is

$$\begin{aligned}\Sigma_\nu(\boldsymbol{k}, \omega_n) = {} & \frac{T}{N}\sum_{\boldsymbol{q},\nu_m}\exp[\mathrm{i}(\nu_m + \omega_n)0^+]\Gamma_{\nu\nu}(\boldsymbol{q}, \nu_m)G_\nu(\boldsymbol{q}+\boldsymbol{k}, \nu_m + \omega_n) \\ & + \frac{2T}{N}\sum_{\boldsymbol{q},\nu_m}\exp[\mathrm{i}(\nu_m - \omega_n)0^+]\Gamma_{\nu\bar{\nu}}(\boldsymbol{q}, \nu_m)G_{\bar{\nu}}(\boldsymbol{q}-\boldsymbol{k}, \nu_m - \omega_n),\end{aligned} \tag{2}$$

where T is the (quasi)temperature, $\omega_n = (2n+1)\pi T$, and $\nu_m = 2\pi m T$ with integer n and m. The symbol 0^+ denotes a time infinitesimally later than $\tau = 0$. Here the spin index σ is omitted because we consider only the spin-symmetric case but the spin weight (a factor of two) is counted. The single-particle Matsubara Green's function $G_\nu(\boldsymbol{k}, \omega_n)$ defined by the Fourier transform of $-\langle T_\tau \hat{a}^{\nu}_{j\sigma}(\tau)\hat{a}^{\nu\dagger}_{j'\sigma}\rangle$ is expressed in terms of the self-energy (2) as

$$G_\nu(\boldsymbol{k}, \omega_n) = \frac{1}{\mathrm{i}\omega_n + \mu_\nu - \epsilon^{\nu}_{\boldsymbol{k}} - \Sigma_\nu(\boldsymbol{k}, \omega_n)}, \tag{3}$$

where $\epsilon^{\nu}_{\boldsymbol{k}}$ is the band dispersion of the noninteracting electrons/holes. The two-particle vertex functions $\Gamma_{\nu\nu'}(\boldsymbol{q}, \nu_m)$ are obtained as $\Gamma_{\nu\nu}(\boldsymbol{q}, \nu_m) = U[1 - UK_{\nu\nu}(\boldsymbol{q}, \nu_m)]^{-1}$ and $\Gamma_{\nu\bar{\nu}}(\boldsymbol{q}, \nu_m) = -U'[1 + U'K_{\nu\bar{\nu}}(\boldsymbol{q}, \nu_m)]^{-1}$, where the pair propagators are $K_{\nu\nu}(\boldsymbol{q}, \nu_m) = -(T/N)\sum_{\boldsymbol{k},\omega_n} G_\nu(\boldsymbol{k}, \omega_n)G_\nu(\boldsymbol{q}+\boldsymbol{k}, \nu_m + \omega_n)$ and $K_{\nu\bar{\nu}}(\boldsymbol{q}, \nu_m) = -(T/N)\sum_{\boldsymbol{k},\omega_n} G_\nu(\boldsymbol{k}, \omega_n)G_{\bar{\nu}}(\boldsymbol{q}-\boldsymbol{k}, \nu_m - \omega_n)$. We combine a local approximation (LA) with the SCTMA to simplify the self-consistent calculation [41]. The procedure is performed by neglecting the momentum dependence of the self-energy and the vertex function, i.e. $\Sigma_\nu(\boldsymbol{k}, \omega_n) \to \Sigma_\nu(\omega_n)$ and $\Gamma_{\nu\nu'}(\boldsymbol{q}, \nu_m) \to \Gamma_{\nu\nu'}(\nu_m)$. The Green's function also becomes local as

$$G_\nu(\omega_n) = \frac{1}{N}\sum_{\boldsymbol{k}} G_\nu(\boldsymbol{k}, \omega_n) = \int \mathrm{d}\epsilon \frac{\rho^0_\nu(\epsilon)}{\mathrm{i}\omega_n + \mu_\nu - \epsilon - \Sigma_\nu(\omega_n)}, \tag{4}$$

with the noninteracting density of states (DOS) $\rho^0_\nu(\epsilon)$.

To determine the condensation temperature T_c of the condensation of e–h pairs, we examine the e–h singlet pair susceptibility $\chi(\boldsymbol{q}, \nu_m)$, defined by the Fourier transform of $-\langle T_\tau \hat{a}^{\mathrm{h}}_{j,-\sigma}(\tau)\hat{a}^{\mathrm{e}}_{j\sigma}(\tau)\hat{a}^{\mathrm{e}\dagger}_{j'\sigma}(\tau')\hat{a}^{\mathrm{h}\dagger}_{j',-\sigma}(\tau')\rangle$, which is given by the ladder terms corresponding to $\Gamma_{\mathrm{eh}}(\boldsymbol{q}, \nu_m)$, i.e.

$$\chi(\boldsymbol{q}, \nu_m) = \frac{K_{\mathrm{eh}}(\boldsymbol{q}, \nu_m)}{1 + U'K_{\mathrm{eh}}(\boldsymbol{q}, \nu_m)}. \tag{5}$$

Within the SCTMA the repulsive interaction U does not appear explicitly in (5), but it influences the e–h pair susceptibility through the single-particle Green's functions. If the uniform static e–h pair susceptibility $\chi(\boldsymbol{0}, 0)$ diverges for $T \searrow T_\mathrm{c}$, it is a signal of the onset

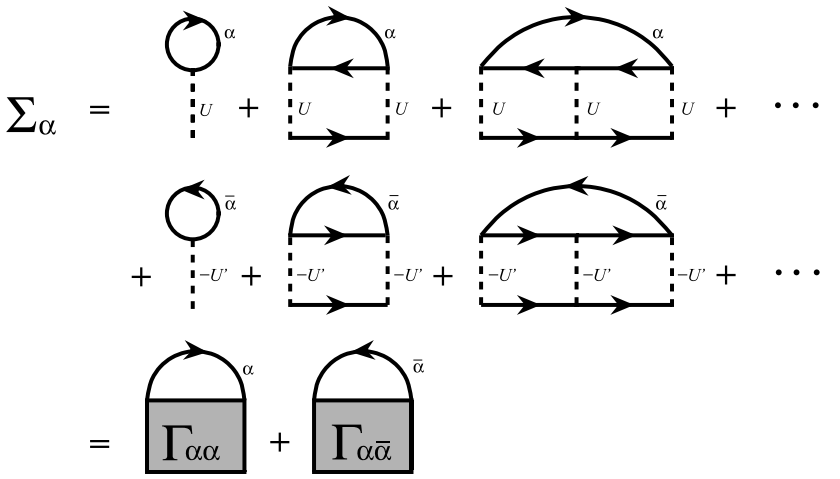

Figure 1. Feynman diagrams for the self-energy in the normal phase. The solid line denotes the electron or hole Green's function G_α, where $\bar{\alpha} =$ h (e) for $\alpha =$ e (h).

of the e–h pair condensation. Thus the condensation temperature T_c can be determined by the condition

$$1 + U' K_{eh}(\mathbf{0}, 0) = 1 - U' T \sum_{\omega_n} \frac{G_e(\omega_n) - \gamma G_h^*(\omega_n)}{\zeta_h^*(\omega_n) - \gamma \zeta_e(\omega_n)} = 0, \tag{6}$$

where $\zeta_\nu(\omega_n) = i\omega_n + \mu_\nu - \Sigma_\nu(\omega_n)$ and $\gamma = t_h/t_e$ is defined as the e–h band mass ratio m_e/m_h. Here we have assumed the relation $\epsilon_{\boldsymbol{k}}^h = \gamma \epsilon_{\boldsymbol{k}}^e$. Hereafter we use $\rho_\nu^0(\varepsilon) = \sqrt{4t_\nu^2 - \varepsilon^2}/(2\pi t_\nu^2)$. The quantity $t_e + t_h$ is taken as the energy unit.

2.2. Condensation temperature

We shall evaluate the condensation temperature T_c from the normal phase to the e–h pair condensed phase. First, we consider the effect of the repulsive interaction U on the condensation temperature T_c. The calculations in this subsection are restricted to the mass ratio $\gamma = 1$. Figure 2 shows the U' dependence of T_c for $U = 0$, 1, and 2 at $n = 0.25$ and $\gamma = 1$. The e–h pair susceptibility in the normal phase diverges for $T \searrow T_c$, which means that the e–h pair condensed phase is realized for $T < T_c$. For $U = 0$, T_c can be described well by the BCS result (dotted curve) in the weak-coupling region ($U' < 0.3$), that is, $T_c \propto \exp(-A/U')$ with a constant A. With increasing U', the solid curve deviates from the BCS result, reaches a maximum at $U' \simeq 1$, and then decreases as $1/U'$ for large U'. The U' dependence of T_c for large U' is related to the behaviour of the BEC temperature of a lattice boson system [31, 32, 40]; the kinetic energy is given by $t_e t_h/U'$ from the virtual pair breaking process. Hence the effective mass $m_e^* + m_h^*$ is proportional to U', which leads to $T_c^{BEC} \sim 1/(m_e^* + m_h^*) \propto t_e t_h/U'$. This result implies the BCS–BEC crossover, as expected. In the presence of U ($U = 1$ and 2), one can see the reduction of T_c for $U' < U$. This fact can be understood as a consequence of the suppression of the excitonic correlation. In contrast, T_c is insensitive to the repulsion U for $U' > U$. This supports the validity of the physical picture of strongly bound e–h pairs that behave almost like neutral bosons for $U' > U$, which is consistent with the behaviour of the density of occupied sites [37].

Next, the effect of the repulsion U on the condensation temperature is examined by changing the e–h particle density n. In figure 3, the U' dependence of T_c at $U = 2$ and

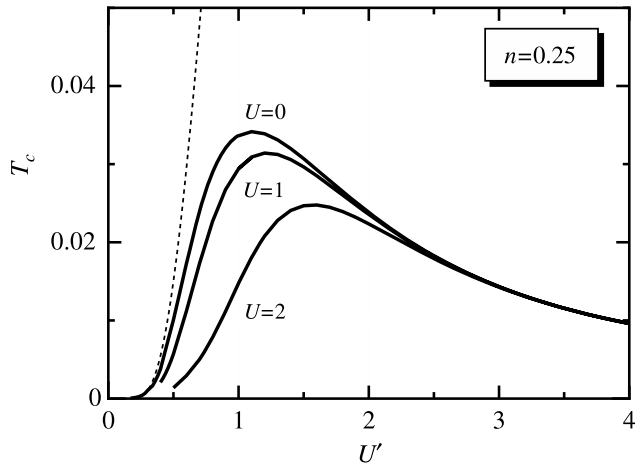

Figure 2. The condensation temperature T_c as a function of U' for $U = 0$, 1, and 2 at $n = 0.25$ and $\gamma = 1$ [37]. The dotted line denotes the result from the BCS theory.

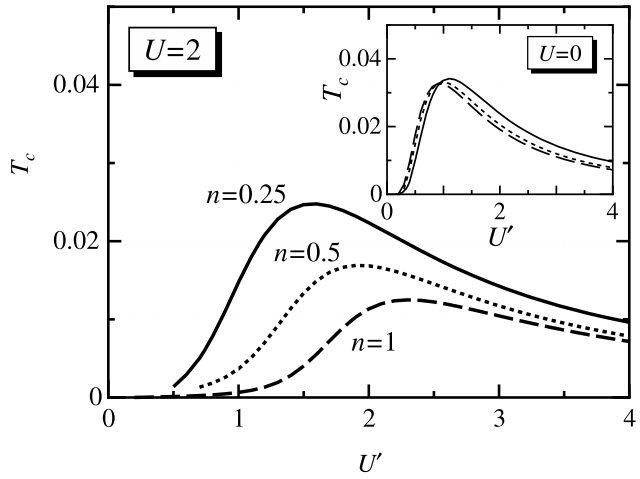

Figure 3. The condensation temperature T_c as a function of U' for $n = 0.25$ (solid line), 0.5 (dotted line), and 1.0 (dashed line) at $U = 2$ and $\gamma = 1$ [37]. The inset shows the case of $U = 0$ for $n = 0.25$, 0.5, and 1.0.

$\gamma = 1$ is shown for $n = 0.25$, 0.5, and 1 (half filling). The inset displays the corresponding U' dependence of T_c for $U = 0$. When $U = 0$, the condensation temperature T_c increases slightly in the weak-coupling region ($U' \ll 1$) as the particle density n is increased. This behaviour is reasonable for $U' \ll 1$ for the following reason. Within the BCS theory the effective attractive interaction between electrons and holes is roughly given by $\rho_\nu^0(\epsilon_F^\nu)U'$, where ϵ_F^ν is the Fermi energy for an uncorrelated system. Hence the effective attraction reaches a maximum when $n = 1$, i.e. the band is half filled, in the case of the semicircular density of states. The presence of U, however, completely changes this tendency. T_c is sufficiently suppressed by U for $U' < U$ as n approaches unity. When we simply consider the effect of U in the BCS regime, the effective interaction $\rho_\nu^0(\epsilon_F^\nu)U'$ could be replaced by $\rho_\nu(\epsilon_F^\nu)U'$, where $\rho_\nu(\epsilon_F^\nu) = -\operatorname{Im} G_\nu(\omega + i0^+)/\pi|_{\omega=\epsilon_F^\nu}$, the interacting DOS at $\omega = \epsilon_F^\nu$, is strongly renormalized

by U [37]. The renormalization becomes strong as n approaches unity [42]. As a result, the effective interaction is reduced by U as $n \to 1$, leading to the suppression of T_c. Meanwhile, for large U' the contribution of U to T_c is very small regardless of the value of n.

The mass difference γ has an effect of reducing the condensation temperature, which is qualitatively consistent with the result of the BCS-like pairing theory [36]. In addition to the reduction of T_c in the weak-coupling BCS regime, our result also involves the suppression of T_c in the strong-coupling BEC regime. Such a behaviour of T_c can be understood analytically in the weak- and strong-coupling limits as follows.

In the weak-coupling limit, the condensation temperature can be estimated by the Hartree term in the self-energy as

$$T_c^{\mathrm{BCS}} = 1.13\sqrt{w_c^e w_c^h}\exp\left[-\frac{t_e + t_h}{2t_\nu \rho_\nu^0(\epsilon_F^\nu)U'}\right], \tag{7}$$

where w_c^ν is a cut-off energy of order ϵ_F^ν. Note that $t_e\rho_e^0(\epsilon_F^e) = t_h\rho_h^0(\epsilon_F^h)$. The effective e–h attractive interaction is given by $t_\nu\rho_\nu^0(\epsilon_F^\nu)U'$. Moreover, the system is characterized by an energy scale $t_e + t_h$ determining the dimensionless effective coupling strength in the weak-coupling region. In our model the quantity $(t_e + t_h)^{-1}$ is proportional to the reduced mass $m_e m_h/(m_e + m_h)$. Therefore, the transition to the e–h pair condensed phase in the weak-coupling region is related to the *relative motion* between electrons and holes, implying the BCS regime. The γ dependence of T_c in the BCS regime can be roughly evaluated from that of the cut-off energy w_c^ν. The cut-off energy of holes w_c^h should be γw_c^e ($\sim\gamma t_e$), since $\epsilon_F^h = \gamma\epsilon_F^e$ ($\sim\gamma t_e$). Thus the coefficient of equation (7) becomes $\sqrt{w_c^e w_c^h} \sim \sqrt{\gamma}t_e$, and so it is found that T_c in the BCS regime would be approximately proportional to $\sqrt{\gamma}/(1+\gamma)$.

On the other hand, in the strong-coupling limit, the model (1) can be reduced to a spinless e–h model:

$$\hat{H} = -\sum_{\langle ij\rangle}\sum_{\nu=e,h} t_\nu \hat{a}_i^{\nu\dagger}\hat{a}_j^\nu - U'\sum_j \hat{n}_j^e\hat{n}_j^h, \tag{8}$$

since the double occupancy at a site by electrons (holes) is forbidden at $U = \infty$. For large U', this model (8) can be mapped to a hard-core boson model with the kinetic energy $2t_e t_h/U'$ and the potential energy $(t_e^2 + t_h^2)/U'$. Using the standard mean-field theory, we can obtain the BEC temperature in the limit of $U \to \infty$ and large U' as

$$T_c^{\mathrm{BEC}} = \frac{2t_e t_h}{U'}\frac{2n-1}{\ln\left[n/(1-n)\right]}. \tag{9}$$

This shows the system is characterized by an energy scale $t_e t_h/(t_e + t_h)$ determining the dimensionless effective coupling strength in the strong-coupling region, which is related to the *motion of the centre of mass* since $(t_e + t_h)/(t_e t_h) \propto m_e + m_h$. The U' dependence of T_c in the strong-coupling region can be described asymptotically in terms of $t_e t_h/U'$. The condensation temperature T_c for various mass ratios γ tends to behave linearly with the slope of -1 (i.e., $T_c \propto 1/U'$) and merges in the large-U' region, implying the BEC regime. As seen from (9), the γ dependence of T_c in the BEC regime is given by $T_c \propto t_e t_h = \gamma/(1+\gamma)^2$. Therefore, it is confirmed that for fixed U' and n the condensation temperature is suppressed by the e–h mass difference in the BEC regime, as well as in the BCS regime. Thus we can emphasize that the excitonic BCS–BEC crossover can be marked by the change of the characteristic energy scale from $t_e + t_h$ to $t_e t_h/(t_e + t_h)$.

3. Exciton Mott transition in high-dimensional e–h systems

The metal–insulator transitions in e–h systems have attracted interest for many years [11]: the exciton Mott transition between an exciton/biexciton gas phase and an e–h plasma phase. Here

we examine the exciton Mott transition in consideration of the minimum elements, i.e. a two-band Hubbard model (1), by using the dynamical mean-field theory (DMFT) [17]. The DMFT requires only the locality of the self-energy, and can take full account of local correlations. This locality and the resulting DMFT become exact in the limit of infinite spatial dimensions and a good approximation of the three-dimensional systems. In this section, we focus on the normal phase, where the condensation of e–h pairs (i.e. exciton BEC and e–h BCS state) is not allowed.

3.1. Dynamical mean-field theory (DMFT)

Within the DMFT [17], the many-body problem of the lattice model, i.e. the two-band Hubbard model (1), is mapped onto the problem of a single-site impurity embedded in an effective medium. The effective medium, which is dynamical and is represented by the noninteracting impurity Green function $\mathcal{G}_0^\nu(\omega)$ of an effective single-impurity Anderson model (SIAM), is determined from the self-consistency condition $\mathcal{G}_0^\nu(\omega)^{-1} = \omega + \mu_\nu - t_\nu^2 G_\nu(\omega)$, where $G_\nu(\omega)$ is the local Green function for electrons or holes of the model (1). The condition is read as $G_{\rm imp}^\nu(\omega) = G_\nu(\omega)$. The interacting impurity Green function of the effective SIAM, $G_{\rm imp}^\nu(\omega)$, should be calculated exactly such that effects of the interactions on the impurity site are fully included. In contrast to the ordinary mean-field approaches, thus, in the DMFT scheme the local correlations and dynamical quantum fluctuations are taken into full account.

In order to extract a sketch of the phase diagram of the model (1), first we apply the two-site DMFT [43]. In the two-site DMFT, the effective medium $\mathcal{G}_0^\nu(\omega)$ is represented approximately by only the fewest parameters, i.e., the effective SIAM consists of a single impurity and only a single bath sites. For the model (1), the corresponding effective two-site SIAM is written as

$$\hat{H}_{\rm imp} = \sum_\sigma \sum_{\nu={\rm e,h}} \left[\varepsilon_{\rm c}^\nu \hat{c}_\sigma^{\nu\dagger}\hat{c}_\sigma^\nu + V_\nu\left(\hat{a}_\sigma^{\nu\dagger}\hat{c}_\sigma^\nu + {\rm h.c.}\right) - \mu_\nu \hat{n}_\sigma^\nu\right] + U\sum_{\nu={\rm e,h}} \hat{n}_\uparrow^\nu \hat{n}_\downarrow^\nu - U'\sum_{\sigma\sigma'} \hat{n}_\sigma^{\rm e}\hat{n}_{\sigma'}^{\rm h}, \tag{10}$$

where the bath parameters V_ν and $\varepsilon_{\rm c}^\nu$ denote the hybridization between the impurity (a) and bath (c) sites, and the energy level of the bath site, respectively. The Green function of the effective medium (i.e. noninteracting impurity Green function) becomes $\mathcal{G}_0^\nu(\omega)^{-1} = \omega + \mu_\nu - V_\nu^2/(\omega - \varepsilon_{\rm c}^\nu)$. In the two-site DMFT, the self-consistency condition is reduced to a simpler equation by the following procedure: the self-energy is expanded in the low-energy region, $\Sigma_\nu(\omega) \sim a_\nu + b_\nu\omega$, and then the resulting local Green function $G_\nu(\omega)$ and impurity Green function $G_{\rm imp}^\nu(\omega) = [\mathcal{G}_0^\nu(\omega)^{-1} - \Sigma_\nu(\omega)]^{-1}$ are compared so as to coincide with each other in the high-energy region. Thereby, the self-consistency equation for V_ν is obtained as

$$V_\nu^2 = t_\nu^2 Z_\nu, \tag{11}$$

where $Z_\nu \equiv (1 - b_\nu)^{-1} = [1 - {\rm d}\Sigma_\nu(\omega)/{\rm d}\omega|_{\omega=0}]^{-1}$ is the quasiparticle weight characterizing the Fermi liquid states. Moreover, the requirement that the particle densities of the original and impurity models must be equal, i.e. $n^\nu = n_{\rm imp}^\nu$, leads to the self-consistency condition for $\varepsilon_{\rm c}^\nu$,

$$\int_{-\infty}^0 {\rm d}\omega\ {\rm Im}\, G_\nu(\omega + {\rm i}0^+) = \int_{-\infty}^0 {\rm d}\omega\ {\rm Im}\, G_{\rm imp}^\nu(\omega + {\rm i}0^+). \tag{12}$$

Evaluating the behaviours of both the quasiparticle weight Z_ν and the interacting DOS $\rho_\nu(\omega)$, we shall discuss the metal–insulator transitions of this system.

3.2. Phase diagram at half filling at zero temperature

First, we concentrate on the special case where both electron and hole bands are half filled, i.e. $n = 1$. In this symmetric case, we can set $\mu_\nu = U/2 - U'$ and $\varepsilon_{\rm c}^\nu = 0$. For $t_{\rm h}/t_{\rm e} = 1$, the

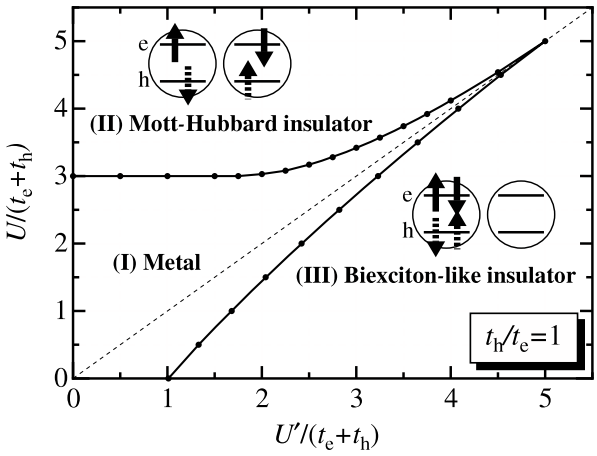

Figure 4. Phase diagram for the exciton Mott transition in the U'–U plane at half-filling ($n = 1$) at zero temperature for $t_h/t_e = 1$ [44].

phase diagram on the plane of U' and U is shown in figure 4. There are three kinds of states: (I) metallic state, (II) Mott–Hubbard insulating state, and (III) biexciton-like insulating state. The second-order transitions among these states occur on the solid curves. In the metallic state (I), Z_ν has a finite value and there is finite DOS at the Fermi level (the quasiparticle coherent peak), i.e. $\rho_\nu(0) \neq 0$. On the other hand, in both insulating states (II) and (III), $Z_\nu = 0$ and the coherent peak of the DOS disappears. However, the physical pictures of the insulating states (II) and (III) are quite different, as drawn schematically in figure 4: state (II) is induced by the e–e (h–h) repulsion U on each electron and hole band, while state (III) is realized by the e–h attraction U' on each site [44]. The competition of these two states stabilizes the metallic state for $U \simeq U'$. These results are equivalent to those obtained for the two-orbital repulsive Hubbard model [45].

We also examine the case of different electron and hole masses. Figure 5 is the phase diagram on the plane of U' and U for $t_h/t_e = 0.5$. A new state (IV) appears between states (I) and (II), in which $Z_e \neq 0$ but $Z_h = 0$, i.e., the electron (hole) band is metallic (insulating). From common features of figures 4 and 5, we find that (i) the metal–insulator transition between states (I) and (III) is by no means 'band selective' for any ratio t_h/t_e and (ii) the position of this phase boundary on the plane of interactions scaled by $t_e + t_h$ is universal with regard to the ratio t_h/t_e. These facts indicate that the transition between the metallic state (I) and the biexciton-like insulator (III) occurs as a result of the competition between the interactions and the relative motion of the electron and hole.

3.3. Phase diagram at arbitrary filling at zero temperature

We discuss the case of arbitrary filling. For $n \neq 1$, the process for determining of the chemical potential μ_ν is added to the self-consistency cycle for ε_c^ν and V_ν. We carried out the exact diagonalization calculation to solve the SIAM instead of the two-site DMFT. Hereafter, $t_h/t_e = 1$ is fixed. The Mott–Hubbard insulator disappears, while the metallic state and the biexciton-like insulator remain. A remarkable feature is the appearance of a new insulating phase, called the 'exciton-like insulator phase', in rather strong repulsion (large U and $U \geqslant U'$). This exciton-like insulator is characterized by $Z_\nu \neq 0$ but $\rho_\nu(0) = 0$ (i.e., a gap opens at Fermi level). In addition, phase transitions among these states are first order;

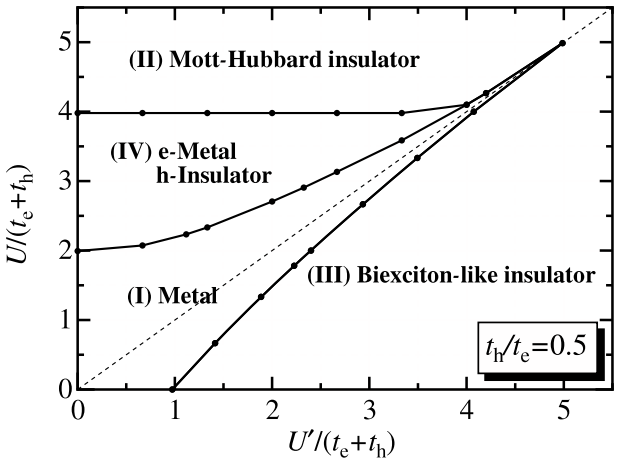

Figure 5. Phase diagram for the exciton Mott transition in the U'–U plane at half-filling ($n = 1$) at zero temperature for $t_h/t_e = 0.5$ [44].

coexisting regions of several phases exist along the phase boundaries. The appearance of the 'exciton-like insulator phase' is understood by considering the limit of $U \to \infty$. In this limit, the model (1) can be mapped onto a single-band attractive Hubbard model with the attraction $-U'$. According to the results of the DMFT study of this model [46, 47], a pairing state appears in addition to the metallic state. This pairing state corresponds to the exciton-like insulating state in our model, in which incoherent local e–h pairs (do not condense) are formed.

Figure 6 shows the phase diagram in the U'–n plane at zero temperature assuming $U = U'$ and $t_e = t_h$. In the metallic phase, the density of states at the Fermi level $\rho_\nu(\mu_\nu)$ is finite (left inset of figure 6) and the quasi-particle weight Z_ν is also finite. On the other hand, an insulating phase, which is characterized by $\rho_\nu(\mu_\nu) = 0$ (right inset of figure 6) and $Z_\nu \neq 0$, is obtained in the wide region for $U' \geqslant 1$ and arbitrary filling. This phase can be assigned as an exciton phase, in which the incoherent local e–h pairs (do not condense) are formed. Indeed, the critical value of $U' = 1$ in the low-density limit $n \to 0$ is given by the binding of a free exciton. The Mott–Hubbard insulator at $n = 1$ for $U = U' \geqslant 5$ could be regarded as the special case ($Z_\nu = 0$) of the exciton phase. The shaded area indicates the coexistent region of the metallic and exciton phases. With varying U' and/or n across the shaded region, one can find the first-order transition between the metallic and exciton phases [48]. Here note that U is not an essential parameter for the transition since the insulating phase at $n \neq 1$ is induced by U'. We also point out that in the case of $U < U'$ a biexciton phase is stabilized instead of the exciton phase.

3.4. Phase diagram at finite temperature

The phase diagram for $n = 0.25$ (one-eighth filling) at finite temperatures is shown in figure 7. In the shaded region ($T \leqslant 0.08$) the metallic and exciton phases coexist. Here it might be a feature of the exciton Mott transition at low density and finite temperatures that the inclination of the phase boundary is opposite to that of the Mott–Hubbard transition. This tendency is reasonable at lower density, because the binding energy of a free exciton is proportional to U' in the model (1) and it corresponds to the phase boundary, i.e., $T \approx U'$, in the low-density limit. Around the shaded region for $T \geqslant 0.08$ the crossover behaviour between the metallic and exciton phases is found. As seen in the inset of figure 7, two branches of Z_ν (solid curves)

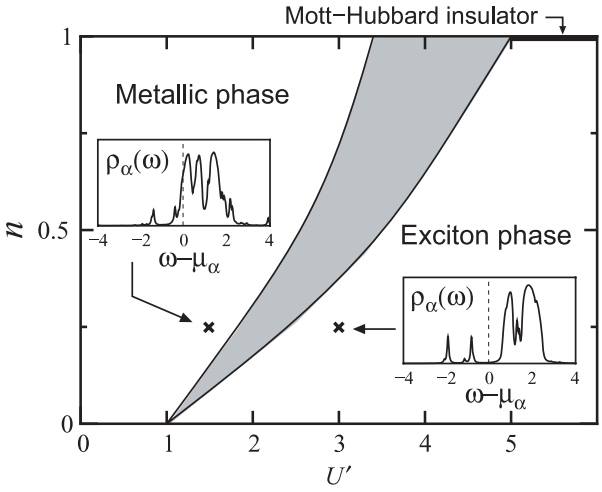

Figure 6. Phase diagram for the exciton Mott transition in the U'–n plane at zero temperature [48]. The left and right insets show the density of states at $n = 0.25$ for $U = U' = 1.5$ and $U = U' = 3.0$, respectively. The shaded area is the coexistent region of the metallic and exciton phases.

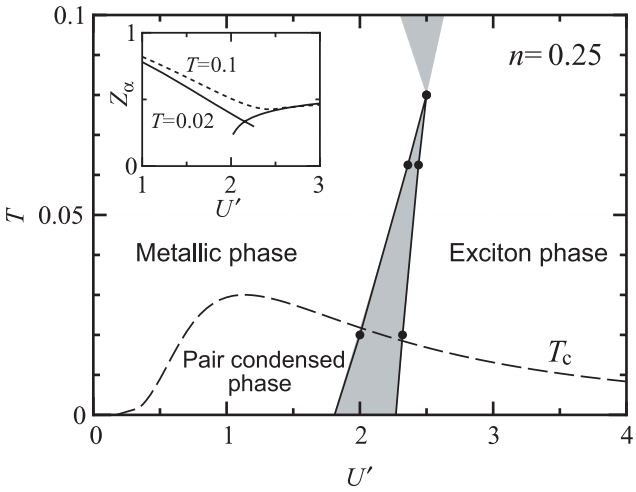

Figure 7. Phase diagram for the exciton Mott transition in the U'–T plane at finite temperature T for $n = 0.25$ [48]. Here $U = U'$ is assumed. The shaded area is the coexistent region of the metallic and exciton phases. The dashed curve is the condensation temperature given in section 2.

merge at high temperature (dotted curve), where the metallic and exciton phases can no longer be distinguished [48].

Our present results will be valid for the intermediate temperatures, i.e. above the condensation temperature T_c of exciton BEC, but below the temperature corresponding to the e–h binding energy E_B. From simple evaluation of T_c and E_B, such a temperature region actually exists: consider again the limit of $U \to \infty$. In the strong limit of U', T_c can be estimated as of order $(t_e + t_h)^2/U'$ [31, 32]. On the other hand, in the low-density limit $n \to 0$, E_B can be estimated as of order U' [32]. Comparing these two characteristic temperatures, such an intermediate temperature region exists even for not so large U' ($\sim t_e + t_h$).

For reference we also plot the condensation temperature (dashed curve in figure 7) of the e–h pair condensation calculated by the SCTMA in section 2. Roughly speaking, T_c (or equivalently the pair condensation gap) is proportional to $\exp(-1/U')$ for $U' \ll 1$ and to $-1/U'$ for $U' \gg 1$. Although a quantitative comparison is not appropriate within the SCTMA calculations, it is expected that for $U' \geqslant 2.5$ phase transition occurs in two stages, i.e. metallic phase (at higher temperatures) $\rightarrow$ exciton phase $\rightarrow$ e–h pair condensed phase (exciton BEC state), and takes place with decreasing T. In the weak-coupling region the direct phase transition between the metallic phase and the e–h pair condensed phase (e–h BCS state) occurs. Detailed analysis is now in progress.

4. Quantum states in one-dimensional e–h systems

We shall consider a high-density electron–hole system in one spatial dimension ($d = 1$). This system is related to semiconductor wire lasers, and then the emergence mechanism of optical gain attracts interest [49]. Since the mean-field approximation is invalid in low dimensions, here we shall make use of the exactly solvable models. We employ the two-band Tomonaga–Luttinger (TL) model [50] to explore the many-body effects in a quasiequilibrium state of electron–hole systems in $d = 1$ [51]. Densities of electrons in the conduction band and holes in the valence band are assumed to be equal to each other (the identical Fermi wavevector $k_F \equiv k_F^e = k_F^h$ for electrons and holes), both of which are high enough that the Fermi points are well defined in both bands.

In this $d = 1$ two-band system, low-energy excitations near each quasi-Fermi level are very important for quantum orderings and their dynamical responses. Then the bosonization method is used to treat the collective excitations of the degenerate electrons and holes. To this end, we linearize the band dispersions near the Fermi points as $\epsilon_\nu(k) \simeq j v_F^\nu (k - j k_F)$ near the right ($j = +1$) and the left ($j = -1$) Fermi points $k = j k_F$. Here $\nu = \{e, h\}$ and the Fermi velocities of the conduction and valence bands are $v_F^e \propto (m_e^*)^{-1}$ and $v_F^h \propto (m_h^*)^{-1}$, respectively. When both bands are far off half filling, the Umklapp processes are negligible. Then the interparticle interaction matrix element is assumed to be spin independent and parametrized to the nine interaction matrix elements: $g_i^e(q)$, $g_i^h(q)$, and $g_i^{eh}(q)$ for $i = 1, 2, 4$, which are momentum dependent in general. In these interaction parameters, g_1 specifies the backward scatterings, which will be discussed in section 4.1. First we study the forward-scattering TL model, which includes essentially only intrabranch, short-range interactions, g_2 (g_2^e, g_2^h, and g_2^{eh}). Next we examine effects of the long-range interaction and the backward scatterings.

4.1. Case of the short-range forward-scattering interaction

According to the bosonization procedure, electron (and hole) field operators can be written in terms of the phase fields, or equivalently boson creation and annihilation operators, e.g.

$$\hat{\psi}_{+\sigma}^e(x) = (2\pi\alpha)^{-1/2} \exp(+ik_F x) \times \exp\left[\frac{i}{2}\left\{\hat{\theta}_e(x) + \hat{\theta}_e^-(x) + \sigma[\hat{\phi}_e(x) + \hat{\phi}_e^-(x)]\right\} + i\hat{\varphi}_{1\sigma}^e\right], \tag{13}$$

$$\hat{\psi}_{-\sigma}^e(x) = (2\pi\alpha)^{-1/2} \exp(-ik_F x) \times \exp\left[-\frac{i}{2}\left\{\hat{\theta}_e(x) - \hat{\theta}_e^-(x) + \sigma[\hat{\phi}_e(x) - \hat{\phi}_e^-(x)]\right\} + i\hat{\varphi}_{2\sigma}^e\right], \tag{14}$$

for the electron fields of branches $j = +1$ and -1, respectively, where α is a cut-off and $\hat{\varphi}_{j\sigma}^e$ is necessary for ensuring the anticommutation relation of $\hat{\psi}_{j\sigma}^e$ with different j and σ. In our definition, $\hat{\psi}_{j\sigma}^h(x)$ annihilates a hole (not an electron) in the valence band of spin σ and

branch j. Using the phase variables, we obtain the phase Hamiltonian of the forward-scattering two-band TL model [52], $\hat{\mathcal{H}} \equiv \hat{\mathcal{H}}_\rho + \hat{\mathcal{H}}_\sigma$, where $\hat{\mathcal{H}}_\rho$ ($\hat{\mathcal{H}}_\sigma$) describes the charge (spin) sector as

$$\hat{\mathcal{H}}_\rho = \int \mathrm{d}x \{A_\mathrm{e}\hat{P}_\mathrm{e}^2(x) + C_\mathrm{e}[\nabla\hat{\theta}_\mathrm{e}(x)]^2 + A_\mathrm{h}\hat{P}_\mathrm{h}^2(x) + C_\mathrm{h}[\nabla\hat{\theta}_\mathrm{h}(x)]^2 + 2C_\mathrm{eh}\nabla\hat{\theta}_\mathrm{e}(x)\nabla\hat{\theta}_\mathrm{h}(x)\}, \tag{15}$$

$$\hat{\mathcal{H}}_\sigma = \int \mathrm{d}x \{B_\mathrm{e}\hat{\Pi}_\mathrm{e}^2(x) + D_\mathrm{e}[\nabla\hat{\phi}_\mathrm{e}(x)]^2 + B_\mathrm{h}\hat{\Pi}_\mathrm{h}^2(x) + D_\mathrm{h}[\nabla\hat{\phi}_\mathrm{h}(x)]^2\}. \tag{16}$$

Here $\hat{\theta}_\mathrm{e}(x)$ ($\hat{\theta}_\mathrm{h}(x)$) is the charge sector of the conduction (valence) electrons, whose conjugate momentum is $\hat{P}_\mathrm{e}(x) \equiv -(4\pi)^{-1}\partial\hat{\theta}_\mathrm{e}^-(x)/\partial x$ ($\hat{P}_\mathrm{h}(x) \equiv -(4\pi)^{-1}\partial\hat{\theta}_\mathrm{h}^-(x)/\partial x$), while $\hat{\phi}_\mathrm{e}(x)$ ($\hat{\phi}_\mathrm{h}(x)$) is the spin phase, whose conjugate momentum is $\hat{\Pi}_\mathrm{e}(x) \equiv -(4\pi)^{-1}\partial\hat{\phi}_\mathrm{e}^-(x)/\partial x$ ($\hat{\Pi}_\mathrm{h}(x) \equiv -(4\pi)^{-1}\partial\hat{\phi}_\mathrm{h}^-(x)/\partial x$). Coefficients are given by $A_\nu \equiv 2\pi(\bar{v}_\mathrm{F}^\nu - g_2^\nu)$, $B_\nu \equiv 2\pi\bar{v}_\mathrm{F}^\nu$, $C_\nu \equiv (\bar{v}_\mathrm{F}^\nu + g_2^\nu)/8\pi$, $D_\nu \equiv \bar{v}_\mathrm{F}^\nu/8\pi$, and $C_\mathrm{eh} \equiv g_2^\mathrm{eh}/4\pi$, where $\bar{v}_\mathrm{F}^\nu \equiv v_\mathrm{F}^\nu + g_4^\nu$ is the normalized Fermi velocity. The charge part of the forward-scattering Hamiltonian, $\hat{\mathcal{H}}_\rho$, is diagonalized by the unitary transformation: $(\hat{\theta}_\mathrm{e}, \hat{\theta}_\mathrm{h}) \to (\hat{\theta}_1, \hat{\theta}_2)$ via

$$\begin{pmatrix} \hat{\theta}_\mathrm{e} \\ \hat{\theta}_\mathrm{h} \end{pmatrix} = \begin{pmatrix} \sqrt{A_\mathrm{e}}\cos\Xi & -\sqrt{A_\mathrm{e}}\sin\Xi \\ \sqrt{A_\mathrm{h}}\sin\Xi & \sqrt{A_\mathrm{h}}\cos\Xi \end{pmatrix} \begin{pmatrix} \hat{\theta}_1 \\ \hat{\theta}_2 \end{pmatrix}, \tag{17}$$

with Ξ being given by $\tan 2\Xi \equiv 2C_\mathrm{eh}\sqrt{A_\mathrm{e}A_\mathrm{h}}/(A_\mathrm{e}C_\mathrm{e} - A_\mathrm{h}C_\mathrm{h})$. Consequently, the diagonalized forward-scattering Hamiltonian becomes

$$\hat{\mathcal{H}}_\mathrm{forward} = \int \mathrm{d}x \sum_{i=1,2} \left\{\hat{P}_i^2(x) + [v_\rho^{(i)}\nabla\hat{\theta}_i(x)]^2\right\} + \hat{\mathcal{H}}_\sigma, \tag{18}$$

where $\hat{P}_i$ is the conjugate momentum for $\hat{\theta}_i$ ($\hat{\mathcal{H}}_\sigma$ is already diagonalized). The motions of four phases, $\hat{\theta}_1$, $\hat{\theta}_2$, $\hat{\phi}_\mathrm{e}$, and $\hat{\phi}_\mathrm{h}$, are described by massless acoustic modes, which have gapless linear dispersions in their excitation spectra. The velocities of the transformed charge phases, $\hat{\theta}_1$ and $\hat{\theta}_2$, are

$$v_\rho^{(i)} = \left\{2(A_\mathrm{e}C_\mathrm{e} + A_\mathrm{h}C_\mathrm{h}) \pm 2\left[(A_\mathrm{e}C_\mathrm{e} - A_\mathrm{h}C_\mathrm{h})^2 + 4C_\mathrm{eh}^2A_\mathrm{e}A_\mathrm{h}\right]^{1/2}\right\}^{1/2}, \tag{19}$$

respectively, where $i = 1$ (2) corresponds to the $+$ ($-$) sign of the right-hand side. On the other hand, velocities of the spin phases, $\hat{\phi}_\mathrm{e}$ and $\hat{\phi}_\mathrm{h}$, are v_F^e and v_F^h, respectively: $v_\sigma^\nu = v_\mathrm{F}^\nu$.

In $d = 1$ quantum many-particle systems, the competition among various Fermi-surface instabilities occurs through quantum fluctuations even at zero temperature. There are 16 possible two-body order parameters, $\hat{\mathcal{O}}(x)$. All the four-body correlation functions, $\langle\hat{\mathcal{O}}(x,\tau)\hat{\mathcal{O}}^\dagger(0,0)\rangle$, behave like $[\max(x,\tau)]^{-\eta}$ for large x and large imaginary time τ. The exponent η for each order parameter is given in [52]. The phase diagram of the quasi-thermal-equilibrium state was given, which is divided into the following four regions [52].

(a) *Exciton BEC phase.* The corresponding two-body order parameter is

$$\hat{\mathcal{O}}_\mathrm{BEC}(x) \equiv \sum_{j=\pm1}\sum_\sigma \hat{\psi}_{j\sigma}^{\mathrm{e}\dagger}(x)\hat{\psi}_{j\mp\sigma}^{\mathrm{h}\dagger}(x). \tag{20}$$

When the repulsive interaction between conduction electrons and valence ones is strong (positive and large g_2^eh), i.e. strong attraction between electrons and holes, the exciton BEC at zero total momentum predominates. Spin-singlet and triplet exciton BECs are degenerate in our spin-independent forward-scattering model. The exciton density wave (EDW) at $\pm2k_\mathrm{F}$ momentum, $\hat{\mathcal{O}}_\mathrm{EDW}(x) \equiv \sum_{j=\pm1}\sum_\sigma \hat{\psi}_{j\sigma}^{\mathrm{e}\dagger}(x)\hat{\psi}_{-j\mp\sigma}^{\mathrm{h}\dagger}(x)$, cannot prevail in the whole plane.

(b) *Density wave phase.* When the repulsion between the electrons within each band is strong (positive and large $g_2^{\rm e}$ or $g_2^{\rm h}$), the ν charge-density wave (ν-CDW) and the ν spin-density wave (ν-SDW) predominate for $\nu = \{e, h\}$. Order parameters of the ν-CDW and ν-SDW are

$$\hat{\mathcal{O}}^{\nu}_{\rm CDW}(x) \equiv \sum_{j=\pm 1}\sum_{\sigma} \hat{\psi}^{\nu\dagger}_{j\sigma}(x)\hat{\psi}^{\nu}_{-j\sigma}(x), \tag{21}$$

$$\hat{\mathcal{O}}^{\nu}_{\rm SDW}(x) \equiv \sum_{j=\pm 1}\sum_{\sigma} \sigma\hat{\psi}^{\nu\dagger}_{j\sigma}(x)\hat{\psi}^{\nu}_{-j\sigma}(x), \tag{22}$$

respectively. The valence-band electrons (i.e. holes) with heavier mass have the stronger tendency toward the ordering. When the velocity ratio $|v_{\rm F}^{\rm h}/v_{\rm F}^{\rm e}|$ is decreased from unity, the h-CDW and h-SDW region extends and invades the exciton BEC region.

(c) *Ordinary intraband superconductivity phase.* The attractive interactions, e.g. negative $g_2^{\rm h}$, yield conventional superconductivity (SC) resulting in intraband pairing with zero total momentum. The order parameter is defined as

$$\hat{\mathcal{O}}^{\nu}_{\rm SC}(x) \equiv \sum_{j=\pm 1}\sum_{\sigma} \hat{\psi}^{\nu}_{j\sigma}(x)\hat{\psi}^{\nu}_{-j\mp\sigma}(x). \tag{23}$$

The valence-band electrons with heavier mass have stronger tendency toward ordering. Singlet and triplet SCs are degenerate.

(d) *Unconventional interband superconductivity phase.* On the other hand, the negative $g_2^{\rm eh}$ causes *interband* Cooper pairing with $\pm 2k_{\rm F}$ momentum:

$$\hat{\mathcal{O}}^{\rm eh}_{\rm SC}(x) \equiv \sum_{j=\pm 1}\sum_{\sigma} \hat{\psi}^{\rm e}_{j\sigma}(x)\hat{\psi}^{\rm h\dagger}_{j\pm\sigma}(x). \tag{24}$$

This unconventional superconductivity is a peculiar feature of $d = 1$ e–h systems. The interband SC with zero total momentum, $\sum_{j=\pm 1}\sum_{\sigma}\hat{\psi}^{\rm e}_{j\sigma}(x)\hat{\psi}^{\rm h\dagger}_{-j\pm\sigma}(x)$, does not appear.

4.2. Relation to the Fermi-edge singularity

We shall discuss the optical absorption spectrum of the degenerate electron–hole system in $d = 1$ [53]. The linear absorption spectrum $W(\omega)$ is related to the Fourier transform of the correlation function, $\langle \hat{P}(t)\hat{P}^{\dagger}(0)\rangle$, where the dipole operator $\hat{P}(t)$ is given by

$$\hat{P}(t) = |M| \int {\rm d}x \sum_{\sigma} \hat{\psi}^{\rm e\dagger}_{\sigma}(x,t)\hat{\psi}^{\rm h\dagger}_{-\sigma}(x,t){\rm e}^{{\rm i}E_0 t}, \tag{25}$$

where M is an interband matrix element (assumed to be constant), $\hat{\psi}^{\nu}_{\sigma}(x,t) = \exp({\rm i}\hat{\mathcal{H}}t)\hat{\psi}^{\nu}_{\sigma}(x)\exp(-{\rm i}\hat{\mathcal{H}}t)$, $\hat{\psi}^{\nu}_{\sigma} = \sum_{j=\pm 1}\hat{\psi}^{\nu}_{j\sigma}$, and E_0 is the energy of the absorption edge in the single-electron picture. The correlation function of the dipole operator contains the correlation function $C_{\rm sBEC}(t) \equiv \langle \hat{\mathcal{O}}_{\rm sBEC}(x,t)\hat{\mathcal{O}}^{\dagger}_{\rm sBEC}(0,0)\rangle$ of the spin-singlet exciton BEC, $\hat{\mathcal{O}}_{\rm sBEC}(x) \equiv \sum_{j=\pm 1}\sum_{\sigma}\hat{\psi}^{\rm e}_{j\sigma}\,\dagger\,(x)\hat{\psi}^{\rm h\dagger}_{j-\sigma}(x)$. For large t, the correlation function behaves like $C_{\rm sBEC}(t) \sim t^{-\eta_{\rm sBEC}}$ with an exponent $\eta_{\rm sBEC}$. This means that the optical spectrum shows the power-law singularity like $W(\omega) \sim (\hbar\omega - \epsilon_{\rm F})^{\beta}\Theta(\hbar\omega - \epsilon_{\rm F})$ in the vicinity of $\epsilon_{\rm F}$, where $\epsilon_{\rm F}$ is the absorption-edge energy and β is the critical exponent: $\beta = \eta_{\rm sBEC} - 2 = \beta^{\rm ex} + \beta^{\rm c-oc} + \beta^{\rm v-oc}$, where

$$\beta^{\rm ex} = -\frac{\pi[v_{\rho}^{(1)} - v_{\rho}^{(2)}]}{2\sqrt{A_{\rm e}A_{\rm h}}}\left[1 + \frac{A_{\rm e}A_{\rm h}}{4\pi^2 v_{\rho}^{(1)}v_{\rho}^{(2)}}\right]\sin 2\Xi, \tag{26}$$

$$\beta^{\rm c-oc} = \frac{A_{\rm h}s_1}{8\pi v_{\rho}^{(1)}v_{\rho}^{(2)}} + \frac{\pi s_2}{2A_{\rm h}} - \frac{1}{2}, \tag{27}$$

$$\beta^{\rm v-oc} = \frac{A_{\rm e}s_2}{8\pi v_{\rho}^{(1)}v_{\rho}^{(2)}} + \frac{\pi s_1}{2A_{\rm e}} - \frac{1}{2}. \tag{28}$$

Here $s_i \equiv \frac{1}{2}[v_\rho^{(1)} + v_\rho^{(2)} \pm (v_\rho^{(1)} - v_\rho^{(2)}) \cos 2\Xi]$ with $i = 1$ (2) corresponding to the + (−) sign. This power-law anomaly in optical spectra near an edge energy is one of the Fermi-edge singularities (FESs).

In e–h systems, the FES exponent β is determined by the correlation exponent, η_{sBEC}, of the singlet-exciton BEC. The divergent edge spectrum (corresponding to $\beta < 0$) can be observed when the electron–hole interaction is attractive ($g_2^{\mathrm{eh}} > 0$ and $g_4^{\mathrm{eh}} > 0$) and for rather weak electron–electron and hole–hole correlations [53]. When the excitons lie completely at the BEC state at zero temperature, an optical spectrum is expected to show a δ-function-like peak if we ignore the quantum fluctuations. Actually, however, quantum fluctuation can never be neglected in $d = 1$ systems and it tends to destroy the exciton BEC. Consequently, the δ-function-like peak spectrum vanishes and is replaced by the power-law peak, which is really the FES and is a remnant of the exciton BEC. In this sense, the FES in e–h systems results from a fluctuating condensed state of many $d = 1$ excitons. Effects of the randomness were discussed in [52, 53].

4.3. Case of the long-range Coulomb interaction: biexciton liquid

We shall consider the case where the interaction potential behaves as unscreened Coulomb potential ($\propto 1/r$) at long interparticle distance r [54]. Hence, the interaction parameters in the g-ology should become momentum dependent. The e–e, h–h, and e–h backward scatterings are also taken into account, and are parametrized as g_1^{e}, g_1^{h}, and g_1^{eh}, respectively. In this subsection, for simplicity, we restrict ourselves to the e–h symmetric case, $v_{\mathrm{F}} = v_{\mathrm{F}}^{\mathrm{e}} = v_{\mathrm{F}}^{\mathrm{h}}$ and $g_i^{\mathrm{e}} = g_i^{\mathrm{h}}$. Due to r^{-1} dependence of the Coulomb interaction, the coupling parameters of the forward scattering show a logarithmic divergence at $q \to 0$ [55]. In fact, they can be approximated in the form of $g_{2,4}^{\mathrm{e}}(q) = g_{2,4}^{\mathrm{h}}(q) \sim g_{2,4} + 2g_0 K_0(|q|d)$ and $g_{2,4}^{\mathrm{eh}}(q) \sim -g'_{2,4} - 2g_0 K_0(|q|d)$ with the modified Bessel function $K_0(x)$ and the effective diameter of the quantum wire d. The coupling constants $g_{2,4}$ and $g'_{2,4}$ specify the short-range part of forward scattering, and $g_0 = e^2/\epsilon\pi v_{\mathrm{F}}$ its long-range part, where ϵ denotes the dielectric constant. On the other hand, the coupling parameters of the backward scattering can be substituted by constants as $g_1^{\mathrm{e}}(q) = g_1^{\mathrm{h}}(q) = g_1$ and $g_1^{\mathrm{eh}}(q) = -g'_1$, because they show no singularity at $q \sim \pm 2k_{\mathrm{F}}$.

We here introduce the phase operators $\hat{\Phi}_\mu^\xi(x)$ and $\hat{\Theta}_\mu^\xi(x)$ ($\mu = \{\rho, \sigma\}$, $\xi = \{+, -\}$) through $\partial\hat{\Phi}_\rho^\pm(x)/\partial x = -\pi \sum_{j\sigma} \hat{\rho}_{j\sigma}^\pm$, $\partial\hat{\Phi}_\sigma^\pm(x)/\partial x = -\pi \sum_{j\sigma} (-1)^{\delta_{\sigma\downarrow}} \hat{\rho}_{j\sigma}^\pm$, $\partial\hat{\Theta}_\rho^\pm(x)/\partial = \pi \sum_{j\sigma} j\hat{\rho}_{j\sigma}^\pm$, $\partial\hat{\Theta}_\sigma^\pm(x)/\partial x = \pi \sum_{j\sigma} j(-1)^{\delta_{\sigma\downarrow}} \hat{\rho}_{j\sigma}^\pm$, where $\delta_{\sigma\sigma'}$ is the Kronecker's delta, $\hat{\rho}_{j\sigma}^\pm = (\hat{\rho}_{j\sigma}^{\mathrm{e}} \pm \hat{\rho}_{j\sigma}^{\mathrm{h}})/2$, and $\hat{\rho}_{j\sigma}^\nu(x)$ denotes the density at position x for the particle $\nu = \{e, h\}$ with indices $j = \pm 1$ and $\sigma = \{\uparrow, \downarrow\}$. It is noteworthy that $\hat{\Phi}_\rho^+$ and $\hat{\Phi}_\rho^-$ are associated with the mass and charge densities (the sum and difference of electron and hole densities), respectively. Then, the g-ology Hamiltonian with the backward scatterings is written as $\hat{H} = \sum_{\mu=\rho,\sigma,\xi=\pm} \hat{\mathcal{H}}_\mu^\xi + \hat{\mathcal{H}}_{\mathrm{bs}}^{\mathrm{intra}} + \hat{\mathcal{H}}_{\mathrm{bs}}^{\mathrm{inter}}$, where

$$\begin{aligned}
\hat{\mathcal{H}}_\mu^\xi &= \frac{v_\mu^\xi}{2\pi} \int \mathrm{d}x \left\{ K_\mu^\xi \left(\frac{\partial\hat{\Theta}_\mu^\xi}{\partial x} \right)^2 + \frac{1}{K_\mu^\xi} \left(\frac{\partial\hat{\Phi}_\mu^\xi}{\partial x} \right)^2 \right\} \\
&\quad + \frac{v_{\mathrm{F}}}{\pi} \int \mathrm{d}x\, \mathrm{d}x' \frac{2g_0\delta_{\xi-}\delta_{\mu\rho}}{\sqrt{(x-x')^2 + d^2}} \frac{\partial\hat{\Phi}_\rho^-(x)}{\partial x} \frac{\partial\hat{\Phi}_\rho^-(x')}{\partial x'}, \\
\hat{\mathcal{H}}_{\mathrm{bs}}^{\mathrm{intra}} &= \frac{v_{\mathrm{F}} g_1}{\pi\alpha^2} \int \mathrm{d}x \cos 2\hat{\Phi}_\sigma^+ \cos 2\hat{\Phi}_\sigma^-, \\
\hat{\mathcal{H}}_{\mathrm{bs}}^{\mathrm{inter}} &= -\frac{v_{\mathrm{F}} g'_1}{\pi\alpha^2} \int \mathrm{d}x \sum_\xi \cos 2\hat{\Phi}_\rho^- \cos 2\hat{\Phi}_\sigma^\xi .
\end{aligned} \tag{29}$$

Here, we used the renormalized velocity $v_\mu^\xi = v_F\sqrt{a_\mu^\xi b_\mu^\xi}$ and coupling constant $K_\mu^\xi = \sqrt{a_\mu^\xi/b_\mu^\xi}$, where a_μ^ξ and b_μ^ξ are given as $a_\rho^\pm \equiv 1+g_4-g_2+g_1/2\mp g_4'\pm g_2'$, $b_\rho^\pm \equiv 1+g_4+g_2+g_1/2\mp g_4'\mp g_2'$, $a_\sigma^\pm \equiv 1+g_1/2$, and $b_\sigma^\pm \equiv 1-g_1/2$. As in (13) and (14), the field operator can be expressed as $\hat\psi_{j\sigma}^\nu(x) = (2\pi\alpha)^{-1/2}\eta_{j\sigma}^\nu \exp[\mathrm{i}j(k_F x + \hat\phi_{j\sigma}^\nu)]$ in terms of the Klein factor $\eta_{j\sigma}^\nu$ and the phase operators $\hat\phi_{j\sigma}^{\mathrm{e}} \equiv \sum_{\xi=\pm}(-\hat\Phi_\rho^\xi - \sigma\hat\Phi_\sigma^\xi + j\hat\Theta_\rho^\xi + j\sigma\hat\Theta_\sigma^\xi)/2$ and $\hat\phi_{j\sigma}^{\mathrm{h}} \equiv \sum_{\xi=\pm}\xi(-\hat\Phi_\rho^\xi - \sigma\hat\Phi_\sigma^\xi + j\hat\Theta_\rho^\xi + j\sigma\hat\Theta_\sigma^\xi)/2$.

If we neglect the intra- and interband backward scattering terms, $\mathcal{H}_{\mathrm{bs}}^{\mathrm{intra}}$ and $\mathcal{H}_{\mathrm{bs}}^{\mathrm{inter}}$, the Hamiltonian is decoupled into four parts, each reduced to the TL form discussed in the previous subsection. In this case, we evaluate the asymptotic behaviour of the various 16-body correlation functions of the form $C(x) = \langle\hat{\mathcal{O}}^\dagger(x)\hat{\mathcal{O}}(0)\rangle$ [55]. We find that the correlation function of

$$\hat{\mathcal{O}}_{\mathrm{BED}}(x) = \hat\psi_{+\uparrow}^{\mathrm{e}\dagger}\hat\psi_{+\downarrow}^{\mathrm{e}\dagger}\hat\psi_{-\downarrow}^{\mathrm{h}\dagger}\hat\psi_{-\uparrow}^{\mathrm{h}\dagger}\hat\psi_{+\uparrow}^{\mathrm{h}}\hat\psi_{+\downarrow}^{\mathrm{h}}\hat\psi_{-\downarrow}^{\mathrm{e}}\hat\psi_{-\uparrow}^{\mathrm{e}} + \mathrm{h.c.} \sim \cos 4\hat\Phi_\rho^-$$

shows the slowest decay. This eight-body operator $\hat{\mathcal{O}}_{\mathrm{BED}}(x)$ appears in the slowly varying $(0k_F)$ component of the biexciton density (BED) operator. The biexciton creation operator here is given as $\hat\psi_\uparrow^{\mathrm{e}\dagger}\hat\psi_\downarrow^{\mathrm{e}\dagger}\hat\psi_\downarrow^{\mathrm{h}\dagger}\hat\psi_\uparrow^{\mathrm{h}\dagger}$ with $\hat\psi_\sigma^{\nu\dagger} \equiv \sum_{j=\pm1}\hat\psi_{j\sigma}^{\nu\dagger}(x)$. This fact shows the strong tendency towards biexciton formation. In this sense, the ground state has a 'biexciton liquid' character in the case of the long-range Coulomb interaction. This is in striking contrast to the short-range case, where the $2k_F$-CDW is dominant.

4.4. Effects of the backward scattering: biexciton crystallization

Next we discuss effects of the backward scattering. Intraband backward scattering is (marginally) irrelevant if the interband scattering is absent. Thus, we can neglect it to investigate the relevancy of the interband backward scattering. We treat the interband backward scattering term in the self-consistent harmonic approximation (SCHA) and the renormalization group (RG) method. Both results show that the interband backward scattering is always relevant, independent of $g_0 > 0$. Because the coupling constant g_1' is renormalized to a large value, $\hat\Phi_\rho^-$ and $\hat\Phi_\sigma^\pm$ are fixed by the condition $\cos 2\hat\Phi_\rho^- = \cos 2\hat\Phi_\sigma^+ = \cos 2\hat\Phi_\sigma^- = \pm1$, which minimizes the interband backward scattering term. This localization of the phases leads to the energy gaps Δ in the excitation modes corresponding to $(\mu,\xi) = (\rho,-)$, $(\sigma,+)$, and $(\sigma,-)$. The point is that the charge excitation, $(\mu,\xi) = (\rho,-)$, has a gap. This results in the system being an insulator even in the high-e–h-density limit, and suggests that the exciton Mott transition is absent at absolute zero temperature in one dimension. There remains a single gapless excitation corresponding to $(\mu,\xi) = (\rho,+)$ since $\hat{\mathcal{H}}_\rho^+$ is decoupled from the other part of the Hamiltonian. As will be mentioned below, its coupling constant K_ρ^+ specifies the power of the algebraic decay of some correlation functions.

Let us discuss the character of the insulating ground state obtained above. To this end, we investigate the asymptotic behaviour of the correlation function $C(x)$. We find two important results. (i) Because the phases $\hat\Phi_\rho^-$ and $\hat\Phi_\sigma^\pm$ are localized, the fluctuations of their conjugate operators $\hat\Theta_\rho^-$ and $\hat\Theta_\sigma^\pm$ diverge. Thus, $C(x)$ decays exponentially if $\hat{\mathcal{O}}(x)$ contains $\hat\Theta_\rho^-$ or $\hat\Theta_\sigma^\pm$. (ii) If $\hat{\mathcal{O}}(x)$ vanishes under the phase-fixing condition, $C(x)$ shows an exponential decay. Owing to these criteria, it is sufficient to consider the following two operators:

$$\begin{aligned}\hat{\mathcal{O}}_{\mathrm{MDW}}(x) &\equiv \sum_{\nu=\mathrm{e,h}}\hat{\mathcal{O}}_{\mathrm{CDW}}^\nu(x)\\ &= \sum_{\nu=\mathrm{e,h}}\sum_{j=\pm1}\sum_\sigma \hat\psi_{j\sigma}^{\nu\dagger}(x)\hat\psi_{-j\sigma}^\nu(x) \sim \cos[2k_F x - \hat\Phi_\rho^+(x)],\end{aligned} \tag{30}$$

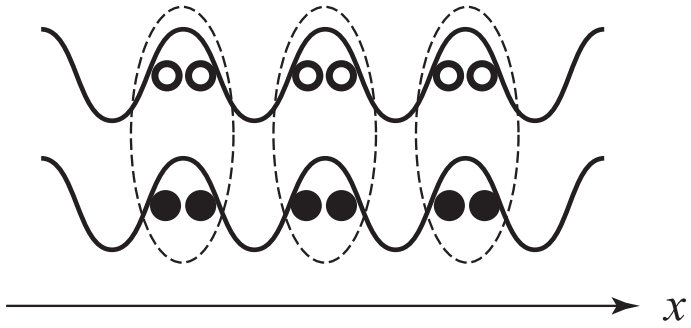

Figure 8. Schematic view of the biexciton crystal. Open (solid) circles mean electrons in a conduction band (holes in a valence band). Two of them get together to form a CDW-like pair in each band. Such pairs of electrons and holes are aligned spatially in phase resulting in the biexciton crystallization (dashed oval lines).

$$\hat{\mathcal{O}}_{\mathrm{BEI}}(x) \equiv \sum_{j=\pm 1}\sum_{\sigma} \hat{\psi}^{\mathrm{e}}_{j\sigma}(x)\hat{\psi}^{\mathrm{e}}_{j-\sigma}(x)\hat{\psi}^{\mathrm{h}}_{-j-\sigma}(x)\hat{\psi}^{\mathrm{h}}_{-j\sigma}(x) \sim \exp[2\mathrm{i}\hat{\Theta}^{+}_{\rho}(x)], \tag{31}$$

where we use the condition $\cos 2\hat{\Phi}^{-}_{\rho} = \cos 2\hat{\Phi}^{+}_{\sigma} = \cos 2\hat{\Phi}^{-}_{\sigma} = 1$. The operator $\hat{\mathcal{O}}_{\mathrm{MDW}}(x)$ denotes the $2k_{\mathrm{F}}$ oscillatory component of the mass density wave (MDW), while $\hat{\mathcal{O}}_{\mathrm{BEI}}(x)$ annihilates a biexciton located at x describing the BEC of biexcitons (biexcitonic insulator, BEI). The asymptotic forms of these correlation functions are

$$C_{\mathrm{MDW}}(x) \sim x^{-K^{+}_{\rho}/2}, \tag{32}$$

$$C_{\mathrm{BEI}}(x) \sim x^{-2/K^{+}_{\rho}}. \tag{33}$$

As a result, the formation of the $2k_{\mathrm{F}}$-MDW or the BEI shows the strongest instability at $K^{+}_{\rho} < 2$ and $K^{+}_{\rho} > 2$, respectively.

In the weak-coupling regime ($g_i \ll 1$ and $g'_i \ll 1$), we obtain $K^{+}_{\rho} \sim 1$, which leads to the strong instability toward the formation of the $2k_{\mathrm{F}}$-MDW. The formation of the $2k_{\mathrm{F}}$-MDW can be interpreted as 'biexciton crystallization'. In fact, the $2k_{\mathrm{F}}$ charge density waves of the electron (e-CDW) and the hole (h-CDW) are simultaneously formed *in an in-phase way* in the $2k_{\mathrm{F}}$-MDW state, since the fluctuation of the total charge density is strongly suppressed. As a result, two electrons and two holes are effectively accumulated to form 'biexcitons' arranged regularly with the periodicity π/k_{F}, as schematically shown in figure 8.

The above discussion is confined to the case of zero temperature. If the temperature $k_{\mathrm{B}}T$ is larger than the energy gap Δ, the effects of the backward scattering terms are negligible. Then, the system shows 'biexciton liquid' character within the length scale $\sim v_{\mathrm{F}}/k_{\mathrm{B}}T$, as discussed in section 4.3. Detailed analysis at finite temperature will be reported in the near future.

5. Concluding remarks

We review recent theoretical results on quantum cooperative phenomena in e–h systems. In particular, the exciton BEC–BCS crossover and the exciton Mott transition in high-dimensional e–h systems, and the biexciton crystallization in one-dimensional e–h systems, are introduced.

By applying the self-consistent t-matrix approximation to the e–h two-band Hubbard model, the condensation temperature to the e–h pair condensed phase is discussed. Analysis in the case of $\gamma \neq 1$ has allowed us to capture the BCS–BEC crossover as the change of the characteristic energy scale from $t_{\mathrm{e}}+t_{\mathrm{h}}$ to $t_{\mathrm{e}}t_{\mathrm{h}}/(t_{\mathrm{e}}+t_{\mathrm{h}})$, where the former is related to the relative

motion and the latter to the motion of the centre of mass. We should mention limitations of the present SCTMA. The n dependence of T_c in the large-U' region is opposite to that of the exact result in the limit of $U \to \infty$ and large U'. The result of figure 3 suggests a decreasing function of n while the exact result is an increasing function of n. Another difficulty is that the SCTMA cannot describe insulating states without any symmetry breaking [42], such as the exciton and biexciton phases. The long-range part of the Coulomb interaction was not considered here. It may become crucial, particularly in the BEC regime.

To clarify how the exciton Mott transition depends on the interaction strengths, a two-band Hubbard model is studied with the dynamical mean-field theory. The phase diagrams in the U–U' and U'–n planes are obtained. When both electron and hole bands are half filled, two types of insulating states appear: the Mott–Hubbard insulator for $U > U'$ and the biexciton-like insulator for $U < U'$. Even when away from half-filling, we find the phase transition between the exciton- or biexciton-like insulator and a metallic state. This transition is found to be the first-order transition. With increasing temperature, this first-order transition continues until the temperature is at a critical point. A detailed phase diagram including quantum condensed states will be reported elsewhere.

Quantum orders of one-dimensional e–h systems are also investigated with the bosonization and the renormalization-group techniques. The systems are insulating even at the high-density limit and the exciton Mott transition never occurs at absolute zero temperature. We find the insulating ground state exhibits a strong instability towards the crystallization of biexcitons.

All the electron–hole issues attracting interest recently are related to quantum many-body problems [56] and/or to nonequilibrium dynamics far from the thermal equilibrium. Not only an electron, a hole, and the mutual Coulomb interaction but also their stage (i.e. dimensionality of the materials) and some supporting players (e.g. phonons, randomness) play interesting roles to yield novel properties. These open new field in photophysics. Moreover, it will be of great interest to use photons not only as a probe for materials but also as a trigger for drastic change and control of the material states including even the ground state [57]. Such photoinduced phase transitions [58, 59] are also a new, promising research field.

Acknowledgments

The works presented in this article have been supported by CREST, JST and Grants-in-Aid from the Ministry of Education, Culture, Sports, Science and Technology of Japan. The authors would like to thank P Huai and H Akiyama for useful discussions. The computation in this work has been done using the facilities of the Supercomputer Centre, Institute for Solid State Physics, University of Tokyo.

References

[1] Ogawa T and Kanemitsu Y 1995 *Optical Properties of Low-Dimensional Materials* (Singapore: World Scientific)
Ogawa T and Kanemitsu Y 1998 *Optical Properties of Low-Dimensional Materials* vol 2 (Singapore: World Scientific)
[2] Haug H and Schmitt-Rink S 1984 *Prog. Quantum Electron.* **9** 3
[3] Zimmermann R 1988 *Many-Particle Theory of Highly Excited Semiconductors* (Leipzig: Teubner)
[4] Göbel E O and Mahler G 1979 *Festkorperprobleme* (*Advances in Solid State Physics* vol XIX) (Braunschweig: Vieweg) p 105
[5] Ogawa T, Furusaki A and Nagaosa N 1992 *Phys. Rev. Lett.* **68** 3638
Otani H and Ogawa T 1996 *Phys. Rev.* B **53** 4684
Otani H and Ogawa T 1996 *Phys. Rev.* B **54** 4540

Ogawa T and Takagiwa M 2002 *Nonlinear Opt.* **29** 465
[6] Ogawa T 2004 *J. Phys.: Condens. Matter* **16** S3567
[7] Ogawa T and Takagahara T 1991 *Phys. Rev.* B **44** 8138
Ohno T, Shiraishi K and Ogawa T 1992 *Phys. Rev. Lett.* **69** 2400
Shimizu A, Ogawa T and Sakaki H 1992 *Phys. Rev.* B **45** 11338
[8] Okumura S and Ogawa T 2002 *Phys. Rev.* B **65** 035105
[9] Okumura S and Ogawa T 2002 *Nonlinear Opt.* **29** 571
[10] Hanamura E and Haug H 1977 *Phys. Rep.* **33** 209
[11] Moskalenko S A and Snoke D W 2000 *Bose–Einstein Condensation of Excitons and Biexcitons* (Cambridge: Cambridge University Press)
[12] Blatt J M, Böer K W and Brandt W 1962 *Phys. Rev.* **126** 1691
[13] Snoke D W 2003 *Phys. Status Solidi* b **238** 389
[14] Snoke D W, Wolfe J P and Mysyrowicz A 1990 *Phys. Rev. Lett.* **64** 2543
Snoke D W, Wolfe J P and Mysyrowicz A 1990 *Phys. Rev.* B **41** 11171
[15] Keldysh L V and Kopaev Y V 1964 *Fiz. Tverd. Tela (Leningrad)* **6** 2791
[16] Jérome D, Rice T M and Kohn W 1967 *Phys. Rev.* **158** 462
[17] Georges A, Kotliar G, Krauth W and Rozenberg M J 1996 *Rev. Mod. Phys.* **68** 13
[18] Ishikawa A, Ogawa T and Sugakov V I 2001 *Phys. Rev.* B **64** 144301
[19] Sugakov V I 1998 *Solid State Commun.* **106** 705
[20] Nazarenko A V, Ogawa T and Sugakov V I 2001 *Phys. Status. Solidi* b **228** 857
[21] Ishikawa A and Ogawa T 2002 *Phys. Rev.* E **65** 026131
[22] Ogawa T, Ishikawa A and Saito S 2006 *J. Lumin.* **119** 188
[23] Wang D W and Das Sarma S 2001 *Phys. Rev.* B **64** 195313
[24] Gogolin A O, Nersesyan A A and Tsvelik A M 1998 *Bosonization and Strongly Correlated Systems* (Cambridge: Cambridge University Press)
[25] Ivanov A L and Haug H 1993 *Phys. Rev. Lett.* **71** 3182
[26] Ivanov A L, Haug H and Keldysh L V 1998 *Phys. Rep.* **296** 237
[27] Comte C and Nozières P 1982 *J. Physique* **43** 1069
[28] Inagaki T J, Aihara M and Takahashi A 2000 *Solid State Commun.* **115** 645
[29] Inagaki T J and Aihara M 2002 *Phys. Rev.* B **65** 205204
[30] Littlewood P B, Eastham P R, Keeling J M J, Marchetti F M, Simons B D and Szymanska M H 2004 *J. Phys.: Condens. Matter* **16** S3597
[31] Nozières P and Schmitt-Rink S 1985 *J. Low Temp. Phys.* **59** 195
[32] Micnas R, Ranninger J and Robaszkiewicz S 1990 *Rev. Mod. Phys.* **62** 113
[33] Randeria M 1995 *Bose–Einstein Condensation* ed A Griffin, D W Snoke and S Stringari (Cambridge: Cambridge University Press) p 355
[34] Ohashi Y and Griffin A 2003 *Phys. Rev.* A **67** 033603
[35] Zittartz J 1967 *Phys. Rev.* **162** 752
[36] Mizoo K, Inagaki T J, Ueshima Y and Aihara M 2005 *J. Phys. Soc. Japan* **74** 1745
[37] Tomio Y, Honda K and Ogawa T 2006 *Phys. Rev.* B **73** 235108
[38] Frèsard R, Glaser B and Wölfle P 1992 *J. Phys.: Condens. Matter* **4** 8565
[39] Haussmann R 1994 *Phys. Rev.* B **49** 12975
[40] Keller M, Metzner W and Schollwöck U 1999 *Phys. Rev.* B **60** 3499
[41] Letz M and Gooding R J 1998 *J. Phys.: Condens. Matter* **10** 6931
[42] Menge B and Müller-Hartmann E 1991 *Z. Phys.* B **82** 237
[43] Potthoff M 2001 *Phys. Rev.* B **64** 165114
[44] Tomio Y and Ogawa T 2005 *J. Lumin.* **112** 220
[45] Koga A, Imai Y and Kawakami N 2002 *Phys. Rev.* B **66** 165107
[46] Keller M, Metzner W and Schollwöck U 2002 *J. Low Temp. Phys.* **126** 961
[47] Capone M, Castellani C and Grilli M 2002 *Phys. Rev. Lett.* **88** 126403
[48] Tomio Y and Ogawa T 2006 *AIP Conf. Proc., Low Temperature Physics: 24th Int. Conf. on Low Temperature Physics* vol 850, p 1313
[49] Huai P and Ogawa T 2006 *J. Lumin.* **119** 468
[50] Tomonaga S 1950 *Prog. Theor. Phys.* **5** 544
Luttinger J M 1963 *J. Math. Phys.* **4** 1154
Haldane F D M 1980 *Phys. Rev. Lett.* **45** 1358
Solyom J 1979 *Adv. Phys.* **28** 201
[51] Tanguy C and Combescot M 1992 *Phys. Rev. Lett.* **68** 1935

Foing J-P, Hulin D, Joffre M, Jackson M K, Oudar J-L, Tanguy C and Combescot M 1992 *Phys. Rev. Lett.* **68** 110
[52] Nagaosa N and Ogawa T 1993 *Solid State Commun.* **88** 295
[53] Ogawa T 1995 *Phys. Status Solidi* b **188** 83
[54] Asano K and Ogawa T 2005 *J. Lumin.* **112** 200
[55] Schulz H J 1993 *Phys. Rev. Lett.* **71** 1864
[56] Ishida K, Aoki H and Ogawa T 1995 *Phys. Rev.* B **52** 8980
[57] Ogawa T 2001 *Phase Transit.* **74** 93
[58] Nasu K 1997 *Relaxations of Excited States and Photo-Induced Phase Transitions* (Berlin: Springer)
[59] Nasu K 2004 *Photoinduced Phase Transitions* (Singapore: World Scientific)